Nuclear constriction segregates mobile nuclear proteins away from chromatin

Jerome Irianto[a,b,†], Charlotte R. Pfeifer[a,b,c,†], Rachel R. Bennett[a,c], Yuntao Xia[a,b], Irena L. Ivanovska[a,b], Andrea J. Liu[a,c], Roger A. Greenberg[a,d], and Dennis E. Discher[a,b,c,*]

[a]Physical Sciences Oncology Center at Penn, [b]Molecular and Cell Biophysics Lab, [c]Graduate Group/Department of Physics and Astronomy, and [d]Cancer Biology, Abramson Family Cancer Research Institute, Perelman School of Medicine, University of Pennsylvania, Philadelphia, PA 19104

ABSTRACT **As a cell squeezes its nucleus through adjacent tissue, penetrates a basement membrane, or enters a small blood capillary, chromatin density and nuclear factors could in principle be physically perturbed. Here, in cancer cell migration through rigid micropores and in passive pulling into micropipettes, local compaction of chromatin is observed coincident with depletion of mobile factors. Heterochromatin/euchromatin was previously estimated from molecular mobility measurements to occupy a volume fraction *f* of roughly two-thirds of the nuclear volume, but based on the relative intensity of DNA and histones in several cancer cell lines drawn into narrow constrictions, *f* can easily increase locally to nearly 100%. By contrast, mobile proteins in the nucleus, including a dozen that function as DNA repair proteins (e.g., BRCA1, 53BP1) or nucleases (e.g., Cas9, FokI), are depleted within the constriction, approaching 0%. Such losses—compounded by the occasional rupture of the nuclear envelope—can have important functional consequences. Studies of a nuclease that targets a locus in chromosome-1 indeed show that constricted migration delays DNA damage.**

Monitoring Editor
Alex Mogilner
New York University

Received: Jun 16, 2016
Revised: Sep 13, 2016
Accepted: Oct 18, 2016

INTRODUCTION

Cells in vivo move through three-dimensional (3D) tissue in many situations. They squeeze into wounds during healing (Clark *et al.*, 1982) and into vessel-adjacent matrix during angiogenesis (Lamalice *et al.*, 2007). Leukocytes migrate through capillaries only 2–3 μm in diameter and contort into sites of injury in response to inflammatory cues (Luster *et al.*, 2005). Embryogenesis requires both progenitor and committed cells to crawl and reposition themselves in developing organs (Kurosaka and Kashina, 2008). Cancer cells invade nearby tissue, penetrate basement membrane barriers, and even enter distant capillary beds during tumor metastasis (Liotta *et al.*, 1991).

As the largest and stiffest organelle (Dahl *et al.*, 2008), the nucleus has long been speculated to sterically limit a cell's ability to migrate through small, stiff pores in tissue matrix (Lichtman, 1970). In migration through 3D fibrous matrix, the nucleus has been described as a "piston" (Petrie *et al.*, 2014), even though pistons are usually considered rigid. Softening the nucleus by lamin-A knockdown indeed enhances the rate of migration through small constrictions for normal human primary cells as well as cancer lines (Shin *et al.*, 2013; Harada *et al.*, 2014). In studying 3D migration, it therefore makes sense to focus on the nucleus—in particular, how its extreme distortion during transit affects chromatin organization and nuclear factors.

Constricted migration of dendritic cells and some cancer lines has been recently reported to cause nuclear envelope rupture, exchange of nucleocytoplasmic proteins, and local enrichments of green fluorescent protein (GFP)–53BP1 suggestive of DNA damage (Denais *et al.*, 2016; Raab *et al.*, 2016). Although many standard markers of breaks need to be examined in such migration, we show here that 53BP1 and other DNA repair factors are frequently heterogeneous within the migrating nucleus and some can even be lost from the nucleus. Loss of 53BP1, which can delay DNA repair, occurs in many tumors of different tissue and cell types—more consistently than either the activation of the repair kinase ATM or appearance of the phosphorylated-histone marker of double-strand breaks γH2AX,

This article was published online ahead of print in MBoC in Press (http://www.molbiolcell.org/cgi/doi/10.1091/mbc.E16-06-0428) on October 26, 2016.

†These authors contributed equally to this work.

*Address correspondence to: Dennis E. Discher (discher@seas.upenn.edu).

Abbreviations used: ATM, ataxia telangiectasia mutated; 53BP1, p53 binding protein 1; BRCA1, breast cancer 1; FRAP, fluorescence recovery after photobleaching; GFP, green fluorescent protein; γH2AX, gamma histone-H2AX; HP1α, heterochromatin protein 1 alpha; NLS, nuclear localization sequence; 4-OHT, 4-hydroxytamoxifen; RPA1, replication protein A1; YFP, yellow fluorescent protein.

and such loss of 53BP1 typically occurs early in carcinogenesis (Ward *et al.*, 2003; Nuciforo *et al.*, 2007). Furthermore, recent study of cancer lines shows that ~20% of migrating cells exhibit new GFP-53BP1 enrichments absent nuclear rupture (Denais *et al.*, 2016; Raab *et al.*, 2016), which implicates processes other than rupture. Here we show that rupture-free squeeze-out of mobile nuclear proteins from a chromatin-rich constriction always occurs within the nucleus, whereas rupture is less frequent. As a functional test, we use an inducible FokI endonuclease model to show that protein squeeze-out—combined with protein mislocalization during rupture—can inhibit DNA damage by a targeted nuclease, consistent with calculations using a phase-separating nucleus model of constricted cell migration.

RESULTS

Unavoidable segregation and occasional rupture

GFP-53BP1 is usually diffuse in the nucleoplasm, consistent with nucleoplasmic mobility (Bekker-Jensen *et al.*, 2005; Pryde *et al.*, 2005). However, during hours-long migration through a 3-μm Transwell, as the nucleus contorts to enter or exit a pore, GFP-53BP1 is less intense within the pore than either DNA or mCherry-histone H2B, which are both enriched in the pore (Figure 1, A and B). Similarly, endogenous 53BP1 (immunostained) and the additional DNA repair factors GFP-Ku70 and -Ku80 (Supplemental Figure S1), all in the mobile phase (Supplemental Table S1), show less intensity within the 3-μm pore than does chromatin, which is an immobile solid phase according to fluorescence recovery after photobleaching (FRAP; Pajerowski *et al.*, 2007). A homogeneously distributed, nucleus localized construct like that used in Raab *et al.* (2016) is also seen to be less intense within 3-μm pores than with the compacted DNA within the same pores (Figure 1, A and B), although such a separation of mobile molecules from immobile ones does not occur within 8-μm pores. Similar results are obtained regardless of whether the mobile molecule is excluded from nucleoli (53BP1 in Supplemental Figure S1) or not (YFP-NLS [yellow fluorescent protein tagged nuclear localization sequence] in Figure 1A). These observations begin to suggest that chromatin is squeezed (like a sponge) as the nucleus is pulled into a small constriction, and this squeezing thereby excludes, and hence depletes, mobile nucleoplasmic factors from the pore.

Protein size or charge could be important, but protein molecular weights vary by sixfold, and charges likely vary from highly anionic to weakly anionic as the isoelectric point (pI) varies from pI ≈ 4.6 for 53BP1 to pI ≈ 5.8 for Ku70 (Supplemental Table S1). To assess the possible effects of local electrostatics, we measured the level of acetylated histone H3 and also found that it was enriched within the 3-μm pores like DNA and histone-H2B (Supplemental Figure S2). In addition to segregation within the nucleus of the mobile proteins, nuclei sometimes rupture during Transwell migration, causing H2B-mCherry, GFP-53BP1, and GFP-Ku70, as well as GFP-Ku80, to leak at least for a few hours into the cytoplasm before ultimately relocalizing in the nucleus (Figure 1, C and D).

Micropipettes have a Transwell-like, cylindrical pore geometry that is well suited to visualizing nuclear mechanics within detached cells whose F-actin cytoskeletons have been disassembled via latrunculin A treatment (Pajerowski *et al.*, 2007). We therefore examined nuclear factor segregation in this reductionist context. Aspiration of many cells shows that GFP-53BP1 always segregates away from the chromatin that condenses within the entrance of a small, 3-μm micropipette (Figure 2A). Of note, segregation of the protein is evident from minute time scales to hour time scales, as is relevant to migration through a Transwell (Figure 1C). These observations begin to suggest a time- and motility-independent mechanism that segregates mobile molecules away from immobile ones.

The various constructs used in migration studies of Figure 1 were imaged in aspiration using smaller or larger micropipette diameters. GFP-53BP1, Ku70, and Ku80 are all strongly excluded from small pipettes (Figure 2Bi), and the YFP-NLS construct is likewise excluded from 3- but not 8-μm pipettes (Figure 2Bii). As with migration through pores, histone-H2B is also not excluded from 3-μm pipettes (Figure 2Biii).

More than a dozen mobile nuclear proteins were expressed as GFP constructs (Supplemental Table S1) and imaged during aspiration. Whereas DNA in all of these cells condensed at the entrance for small pipettes (Figure 2Ci), all mobile proteins indeed segregated like GFP-53BP1, as quantified by the ratio of each protein's intensity inside the pipette entrance to its intensity outside the pipette (Figure 2Cii). Protein molecular weights vary by sixfold, and protein charges likely vary from highly anionic to cationic as the isoelectric points vary from pI ≈ 4.6 for 53BP1 to pI ≈ 7.8 for dCas9 (Supplemental Table S1). Upstream DNA damage-response factors such as MRE11 and RPA1 (Hass *et al.*, 2012), as well as downstream factors such as BRCA1 (Li and Yu, 2013), Ku70, and Ku80, all diminish within an ~3-μm pore. The mobile proteins studied also include a transcription factor (RelA), an epigenetic factor (Sirt6), and the gene-editing nuclease Cas9. Chromatin condensation near the entrance of the constriction—as signified by the intensity ratios for histone H2B and heterochromatin protein HP1α (Figure 2D) in addition to DNA (Figure 2Ci)—is also quantitatively similar to that observed during Transwell migration. Among all of the aspirated cells, 90–95% exhibit this squeeze-out behavior with compressed DNA (Supplemental Figure S3), and the exceptions appear within statistical uncertainty of doing the same. Segregation is thus an inevitable effect of nuclear squeezing.

Segregation is also highly sensitive to pore diameter. Protein intensity ratios decrease with decreasing pipette diameter. Of importance, the protein ratio decreases to zero—signifying total squeeze-out—at an extrapolated critical diameter of ~2 μm (Figure 2C). At that same critical diameter, the DNA intensity ratio should also level off as the chromatin becomes maximally compacted inside the pipette; such a plateau is indeed suggested by the increasingly shallow fit lines between statistically significant DNA ratio data points. In the opposite limit, since both the DNA and protein intensity ratios approach 1.0 above a threshold pipette diameter of ~5 μm, the DNA and protein flow almost equally into such large pores. It is unsurprising, then, that Transwell pores and pipettes with large diameters (~8 μm) do not cause significant condensation of DNA in the pore, nor do they induce segregation of YFP-NLS (Figure 1A). The DNA and protein intensity ratios finally reach 1 at diameter of ~10 μm (Figure 2C). Furthermore, these ratios exhibit the negative linear correlation that one would expect given that chromatin occupies a solid volume fraction f of the nucleus, whereas mobile proteins occupy the free volume $1 - f$ (Figure 2E).

Whereas segregation always occurs within a constricted nucleus, large extension into a 3-μm micropipette sometimes also gives rise to rupture like that of the segregated GFP-53BP1 (Figures 2A and 3A), which leaks over hours (Figure 3B). Rupture and loss of histone-H2B is twofold to threefold less likely than loss of the mobile factors (Figure 3A), consistent with strong binding of H2B to DNA. For other cancer cell types, a physically unavoidable steric exclusion mechanism would be expected to and indeed does apply to GFP-53BP1 segregation and loss in rupture upon aspiration (Figure 3C): these other cell types include the mouse liver cancer line EC4 and wild-type and lamin-A–knockdown A549 cells. The latter results hint

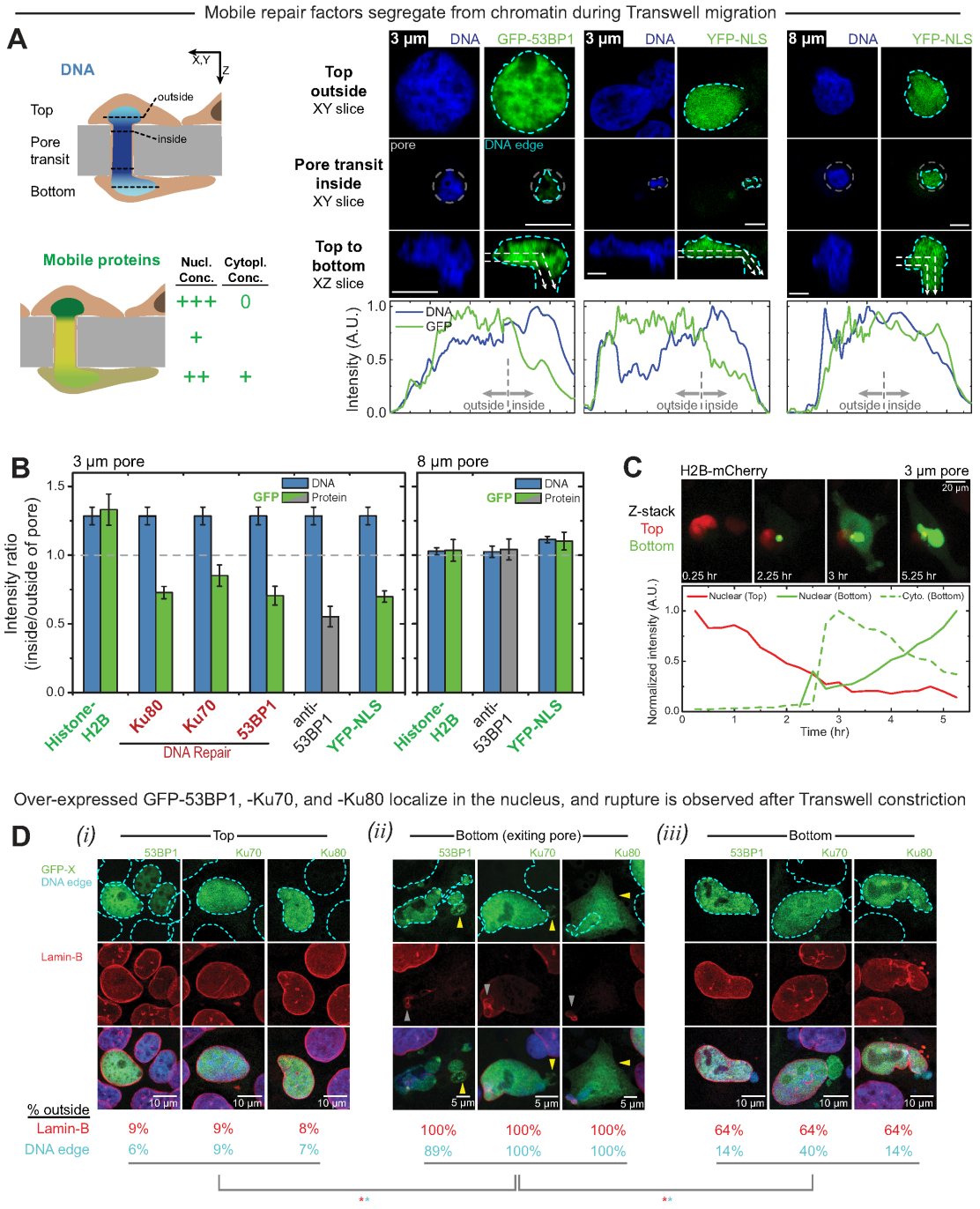

FIGURE 1: Migration through small pores compacts the chromatin and causes local depletion of mobile nuclear proteins plus occasional nuclear rupture. (A) Schematics illustrate that as a cell nucleus squeezes into a small pore, its chromatin becomes compact, and the opposite occurs with mobile proteins. Confocal sections of fixed cells show the same as a nucleus squeezes into a 3-µm pore, with mobile proteins such as GFP-53BP1 and YFP-NLS-MS2 decreasing in density within the small pore (representative of ≥20 cells/protein). Pore exits show similar differences. Large pores of 8 µm show no such DNA compaction or protein depletion. Intensity profiles for DNA and protein are each normalized to the highest values along the dashed arrows shown in the *XZ* slices (bar, 5 µm). (B) Segregation of mobile proteins, including endogenous 53BP1, away from chromatin is evident at both the entrance and exit of 3-µm pores. Because DNA is enriched inside the pore, its intensity ratio tends above 1; the same applies for histone-H2B. Conversely, mobile proteins accumulate outside the pore, so their intensity ratios fall consistently below 1. Segregation does not occur in 8-µm pores (≥20 cells/group, at least three experiments). (C) Live imaging of H2B-mCherry–overexpressing U2OS cells reveals nuclear rupture—with leakage of H2B into the cytoplasm—followed by nuclear relocalization over hours (representative of at least three experiments). (D) At the top and bottom of a Transwell membrane, GFP-53BP1, -Ku70, and -Ku80 localize in the nucleus. For cells exiting 3-µm pores, rupture is sometimes evident with mobile proteins in the cytoplasm based on GFP proteins outside the boundary of lamin-B (red) and/or the DNA edge (blue) (≥9 exiting cells/group, ≥100 top cells/group; $*p < 0.05$). The percentage of cells with mislocalized GFP protein is likewise significantly greater for exiting cells than for cells that fully migrated to the bottom (≥35 bottom cells/group; $*p < 0.05$).

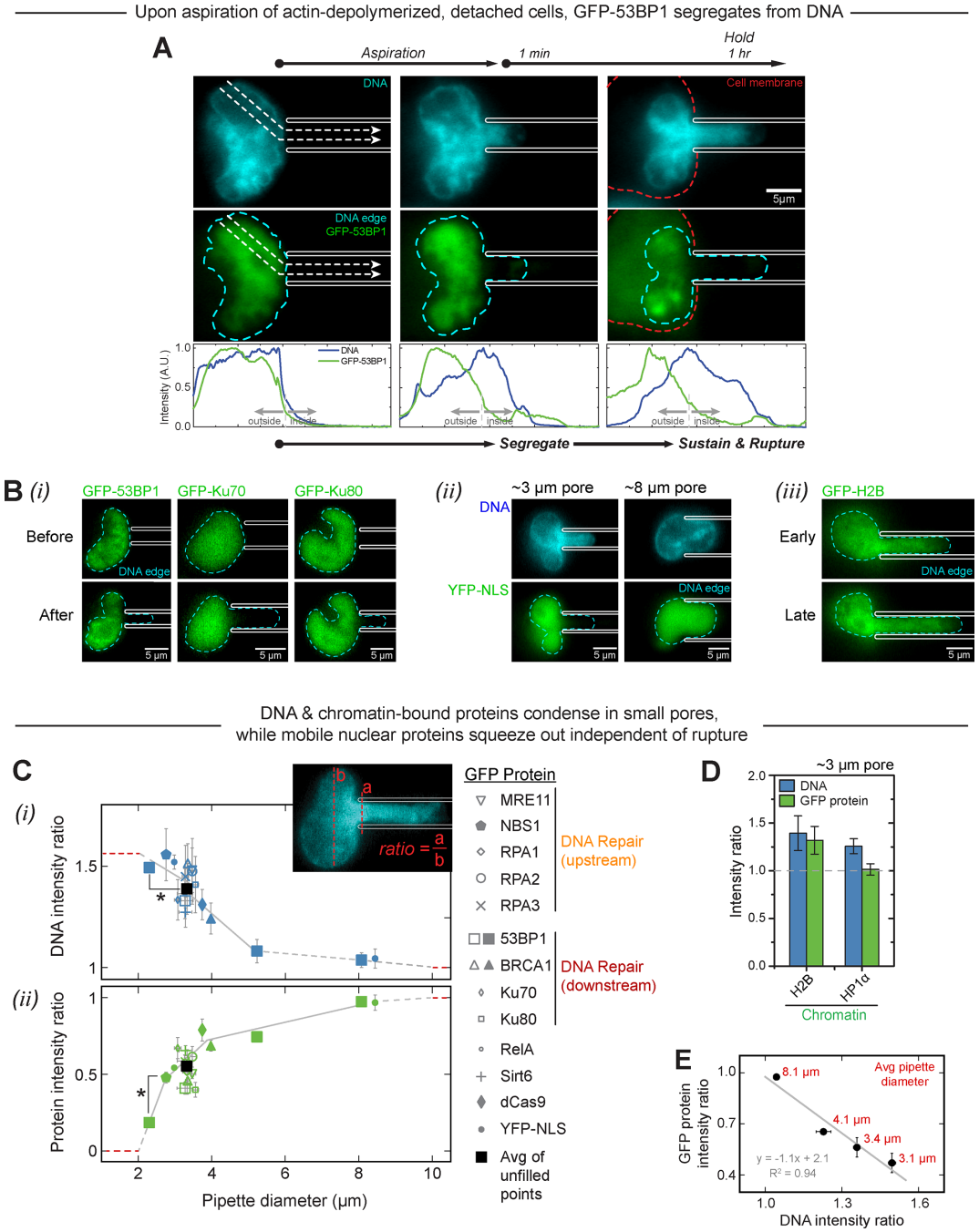

FIGURE 2: Pulling nuclei into small micropipettes consistently compacts the chromatin and causes complementary protein segregation. (A) Cells used for aspiration are deadhered and treated with latrunculin A to depolymerize the cytoskeleton. When a cell and nucleus are then aspirated into a 3-μm pipette, chromatin intensity increases at the pipette entrance and mobile GFP-53BP1 decreases, sometimes leaking or rupturing out of the nucleus. Intensity profiles are shown along the dashed arrows (representative of at least three experiments). (B) Segregation of other mobile GFP proteins contrasts with a DNA-like profile for histone-H2B. (C) All other mobile proteins studied—including repair, transcription, and epigenetic factors, as well as a nuclease—also segregate upon aspiration into ~3-μm pipettes (≥3 cells/group). Segregation is sensitive to pipette size: protein intensity ratio decays with decreasing diameter, vanishing at an extrapolated critical diameter of ~2 μm. Below this critical value, the DNA intensity ratio plateaus as DNA reaches maximum compaction inside the pipette. Unfilled data points fall between 3.0 and 3.7 μm in diameter; their average is indicated by a filled black square. Solid gray lines are fits between filled points with statistically different intensity ratios, and dashed gray lines are extrapolations or fits between points that are not statistically different. YFP-NLS-MS2 was added after the fits but confirms expectations. Red dashed lines show the intensity ratio limits for small and large pipette diameter. (D) Chromatin-bound proteins do not segregate from DNA in ~3-μm pipettes (≥4 cells/group). (E) A negative linear correlation between protein intensity ratio and DNA intensity ratio is consistent with chromatin occupying a solid volume fraction *f* of the nucleus while mobile proteins occupy the free volume 1 – *f* (see *Image analysis* in *Materials and Methods*). Data from C were binned according to average pipette diameter.

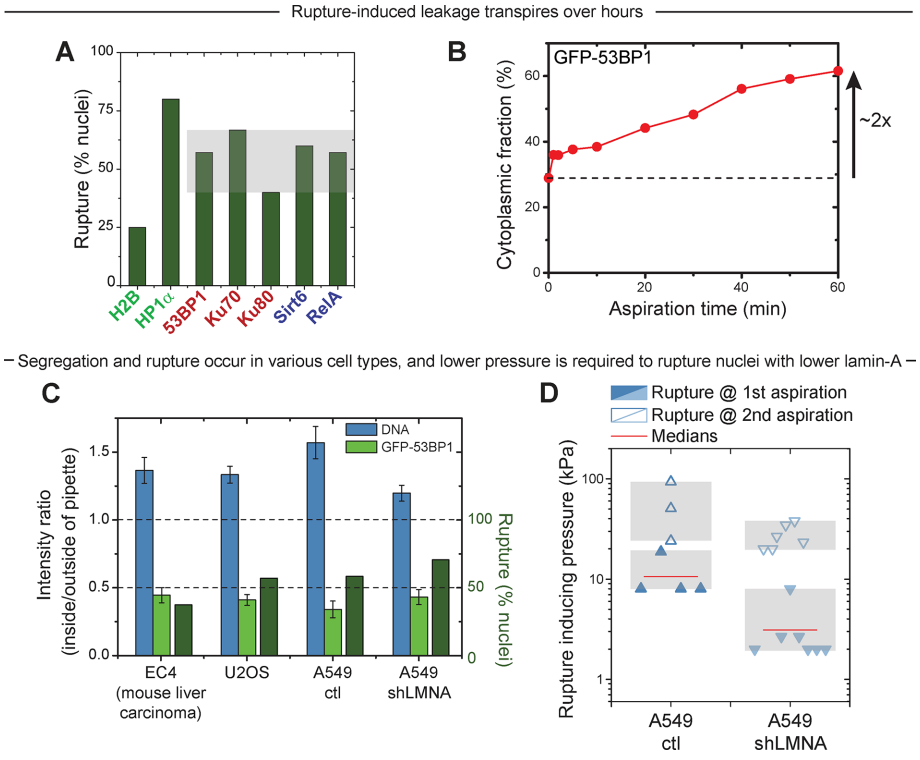

FIGURE 3: Occasional nuclear rupture in aspiration is made easier by knockdown of lamin-A. (A) Nuclear rupture is often observed during aspiration into ~3 μm pipettes. Gray box indicates the range of rupture frequencies for non–chromatin-bound mobile proteins (≥10 cells/group; at least three experiments). (B) During aspiration of a representative cell overexpressing GFP-53BP1, the mobile protein leaks steadily into the cytoplasm. The intensity of 53BP1 in the cytoplasm and in the nucleus was measured over time. Reported is the percentage of total 53BP1 found outside the nucleus—that is, the cytoplasmic fraction—as a function of aspiration time. The cytoplasmic fraction roughly doubles over the course of an hour. (C) Aspiration leads to segregation and rupture of GFP-53BP1 in other cell types, as well: specifically, A549 human lung cancer cells and EC4 mouse liver cancer cells. The percent of nuclei that rupture is shown in dark green (≥10 cells/group; at least three experiments). (D) With lamin-A knockdown, lower pressure is required to induce nuclear rupture. During a typical aspiration experiment, an initial low pressure (~10 kPa) is applied to the nucleus for a sustained period, after which the pressure is increased (to ~50 kPa) if the nucleus has not yet been fully aspirated. The stages are referred to as first and second aspiration, respectively.

at more rupture events with low lamin-A, which prompted a careful examination of rupture as a function of aspiration stress and time course. That lower pressure is required for rupture of lamin-A–knockdown nuclei (Figure 3D) indicates a protective role for lamin-A even on the time scale of minutes-long aspiration. Combined with exclusion from the pore, these findings are all consistent with squeeze-out and overall loss of mobile factors from the DNA compressed into the pore.

Nuclease inhibition by chromatin constriction

Loss of mobile factors during constricted migration should have functional consequences for the cell, such as the delay of DNA damage by nucleases. To investigate this effect, we used a U2OS subline that was engineered to have on/off-inducible DNA damage in ~200 sites in one p-arm locus of chromosome 1 (Figure 4A; Shanbhag *et al.*, 2010; Tang *et al.*, 2013). Cleavage of this locus—by the mCherry-tagged FokI nuclease construct—is induced by the addition of tamoxifen, which translocates the FokI construct into the nucleus (through dimerization), along with Shield1, a stabilizing ligand that prevents FokI degradation. Even in two-dimensional (2D) culture, this damage induction produces the expected correlations 1) between nuclease intensity and intensity of the phosphorylated-histone marker of double-strand breaks γH2AX at the chromosome 1 locus, and 2) between the projected areas of the DNA damage response factor GFP-53BP1and γH2AX at this large locus (DNA length is ~600 μm). Note that whenever mCherry-FokI is detectable as a focal spot, so are the repair factors. A standard electrophoretic "comet assay" further shows that the controlled cleavage of DNA by the nuclease produces a large and expected shift in the DNA centroid toward the cathode in the majority of nuclei from 2D cultures (Figure 4B).

FRAP shows that nucleoplasmic mCherry-FokI is highly mobile (Figure 4C), with a half-life of ~6 s, similar to other constructs (Supplemental Table S1), whereas chromatin-bound FokI is also mobile but with a significantly longer half-life of >2 min. The recovery of the chromatin-bound FokI indicates an exchange between FokI comprising foci and the nucleoplasmic FokI pool. Of importance, FokI is seen to segregate out of both micropipette and Transwell constrictions, decreasing within the pore by ~50% in both cases (Figure 4, D and E). These two different experiments give the same quantitation for DNA and FokI ratios even though they respectively use 1) unfixed versus fixed samples, 2) glass pipettes versus plastic Transwells, 3) single-frame epifluorescence imaging versus slices from confocal stacks, and, of course, 4) different sample orientations with respect to the optical axis. Rupture after Transwell migration is also seen with a similar level of mislocalization by ~50% of FokI into the cytoplasm (Figure 4F). The fact that both segregation and mislocalization after rupture reduce the density of nucleoplasmic FokI per total DNA by a similar amount suggests that their effects should also be similar. Indeed, through both of these mechanisms, constricted migration should dampen FokI nuclease activity on the specially engineered chromosome 1 locus.

Once FokI nuclease has been activated—by high (1 μM) tamoxifen and high (1 μM) Shield1—to cleave the chromosome 1 locus, the percentage of U2OS nuclei with mCherry-positive foci decreases over 24 h even as the nuclease remains abundant within the nucleus (Figure 5, A–C, and Supplemental Figure S4). Reducing the tamoxifen concentration from high to low (0.1 μM) to zero slows this decay by simply reducing the amount of FokI that translocates into the nucleus (Figure 5C). Reactivation with high tamoxifen after 24 h does not fully recover the FokI foci–positive population, indicating that the nuclease causes irreversible cleavage or "burnout" of the locus. After reactivation, the initially zero- and low-tamoxifen groups consistently exhibit a higher percentage of FokI foci–positive cells than the chronically high-tamoxifen group (Figure 5B). Thus transient reduction in the amount of nuclear FokI, followed by restoration of high nuclear FokI levels, results in less burnout than does a sustained high level of the nuclease.

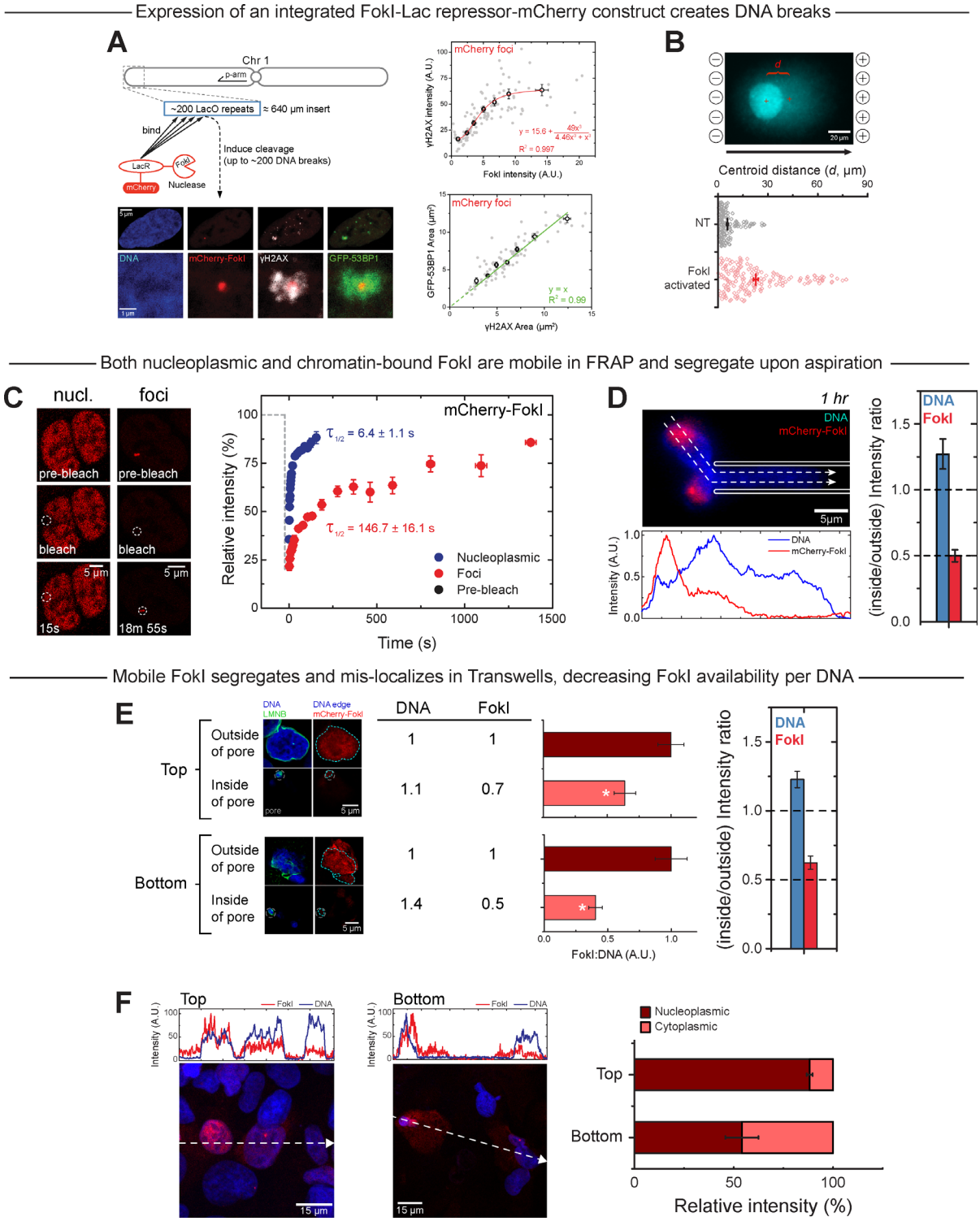

FIGURE 4: FokI nuclease is confirmed to enact on/off-inducible damage at a specific locus on chromosome 1 and also to segregate/mislocalize during Transwell migration. (A) A lac operator transgene integrated into the p-end of chromosome 1 in the U2OS line. Expression of the integrated mCherry-Lac repressor-FokI construct can be stably induced with 4-OHT (tamoxifen) and Shield-1 to creates DNA breaks. FokI intensity correlates with γH2AX intensity, and the area of GFP-53BP1 at the damaged site is linearly correlated to γH2AX focus area. (B) A comet assay is sensitive enough to detect induced DNA breaks: the mean centroid distance is higher for FokI-activated cells (≥175 nuclei/group; at least three experiments). (C, D) FRAP shows that both nucleoplasmic and chromatin-bound mCherry-FokI are mobile, with half-lives of 6 s and >2 min, respectively. The former is thus much more mobile, and it indeed segregates outside a micropipette in D during aspiration (≥4 cells/group; at least three experiments). (E, F) Migration through 3-µm Transwell pores also causes FokI to segregate and mislocalize, as seen in migrated cells that have been fixed for confocal imaging. Intensity profiles are shown along the dashed arrows (>10 cells/group; at least three experiments).

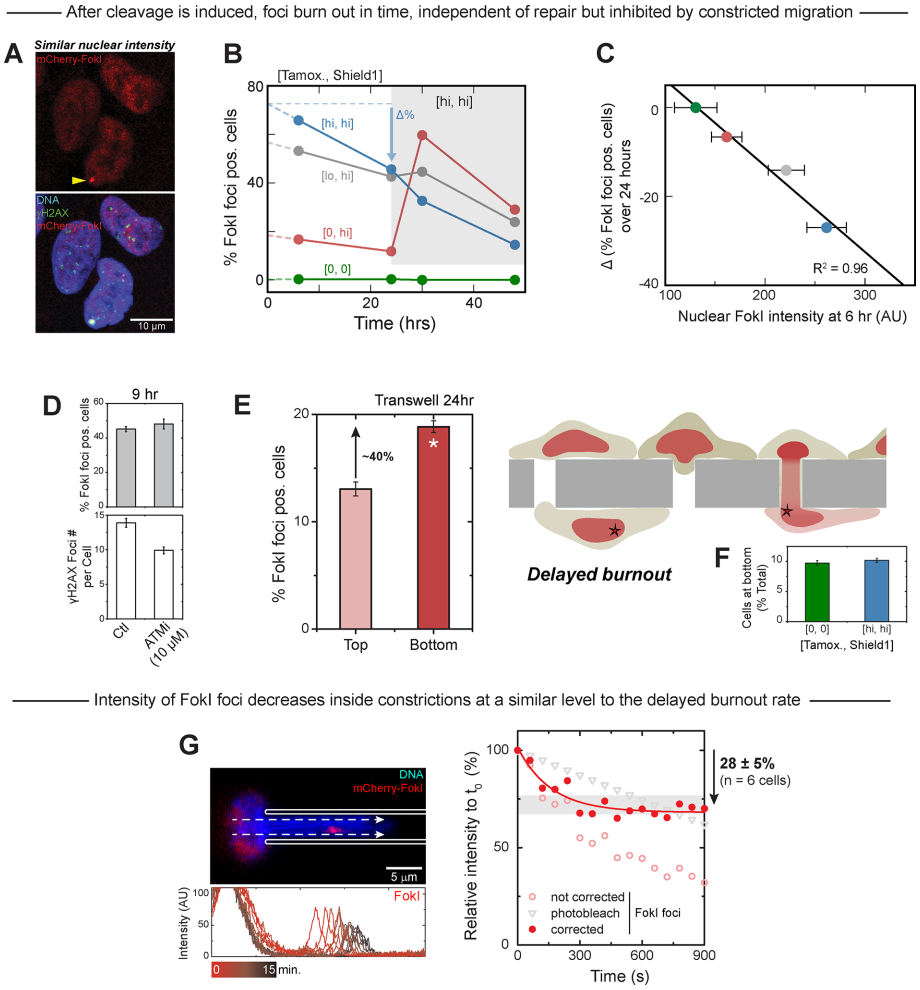

FIGURE 5: Constricted migration—but not repair inhibition—affects a FokI-cleaved locus on chromosome 1. (A–C) FokI cleavage of the engineered chromosome 1 locus is induced at 0 h by controlled addition of two components (tamoxifen, Shield1). High tamoxifen (1 μM, blue) yields a greater percentage of cells positive for mCherry-FokI foci at 6 h than either low (0.1 μM, gray) or zero (red) tamoxifen. In the absence of both inducing chemicals (green), zero foci develop. For all three high-Shield1 groups (1 μM), the percentage of foci-positive cells decreases between 6 and 24 h even as the nucleoplasmic mCherry signal remains strong, indicating "burnout" of the LacO target site by the nuclease. At 24 h, the FokI construct is reactivated with high tamoxifen in all three high-Shield1 groups. Whereas the high-tamoxifen group continues to burn out as before, there are spikes in FokI foci–positive cells for the low- and zero-tamoxifen groups. The burnout rate between 6 and 24 h is used to extrapolate the percentage of FokI foci–positive cells at 0 h, which is, in turn, used to calculate the change in the percentage of foci-positive cells over 24 h. This Δ% defined in B increases in magnitude with nuclear FokI intensity. Hence high tamoxifen (blue) leads to high nuclear FokI levels and correspondingly greater burnout. Low (gray) and zero (red) tamoxifen, as well as zero tamoxifen/Shield1 (green), show less nuclear FokI and less burnout. At least three experiments. (D, E) Inhibition of ATM kinase, which phosphorylates H2AX to make γH2AX, decreases, as expected, the small mCherry-negative focus numbers per cell, but it does not decrease FokI focus numbers. Burnout is thus limited by nuclease induction rather than by repair. Constricted migration through 3-μm Transwells leads to ~40% more cells with FokI foci on the bottom than on top (at least three experiments), which suggests that mobile protein loss during migration impedes targeted FokI activity and so delays burnout. (F) Compared to the nontreated cells, activation of FokI expression by 1 μM tamoxifen and 1 μM Shield1 does not impede migration, as shown by the number of migrated cells at the bottom of the Transwell (≥3 Transwells for each group, at least three experiments). (G) A FokI focus drawn into a 3-μm pipette loses ~30% (≥6 cells) of its initial intensity within minutes, with suitable correction for constant photobleaching.

Inhibition of the DNA damage response using an inhibitor of ATM kinase (Hickson *et al.*, 2004) significantly decreases the number of γH2AX foci—which is expected, since ATM phosphorylation of H2AX, among many targets, generates γH2AX (Shanbhag *et al.*, 2010)—but the inhibition has zero effect on the number of cells with mCherry-FokI foci (Figure 5D). Although segregation of repair factors (Figure 1) could conceivably lead to differences in percentage of foci-positive cells among migrated and nonmigrated populations, burnout of the engineered locus is clearly limited by nuclease activity rather than DNA repair. When induced cells are placed on top of a Transwell membrane, constricted migration to the bottom delays burnout of the locus, with almost 50% more mCherry-positive FokI nuclease foci than on top (Figure 5E). The first possible explanation that we considered was that damage impedes migration, but nuclease induction has no effect on the percentage of cells that migrate (Figure 5F). However, FokI does segregate in constrictions (Figure 4D), draining the nucleoplasmic pool available for exchange with FokI foci (Figure 4C). Indeed, the photobleach-corrected intensity of a FokI focus decreases by ~30% (≥6 cells) within minutes inside a 3-μm constriction (Figure 5G), which coincides with the exchange rate shown by the FRAP experiments (Figure 4C). We considered the possibility that compacted chromatin in the constriction at the specially engineered locus would accumulate (or deplete) core histones. However, histone-H2B remains nearly unperturbed by the FokI locus and nearly constant in intensity (Supplemental Figure S5, 2Biii) even though small changes with this histone will be difficult to resolve because it binds adjacent unaffected chromosomes, which contribute a high background. In two-dimensional cultures, even a temporary decrease in nucleoplasmic FokI can delay burnout considerably (Figure 5, B and C). Segregation and mislocalization of mobile nuclear factors away from chromatin could therefore explain how constricted migration inhibits highly targeted nuclease activity.

DISCUSSION

Migration of immune cells through narrow channels with square cross sections has been seen to draw in the DNA (Thiam *et al.*, 2016), and an increase in nuclear rupture with channel width particularly after lamin-A knockdown (Denais *et al.*, 2016; Raab *et al.*, 2016) could relate somehow to the chromatin compaction in cancer cells shown here in circular pores to hit a steric limit. A first, simple model for squeeze-out of mobile nuclear factors explains the segregation data well and provides a mechanistic basis for our hypothesis that severe constriction can impede targeted nuclease activity. Chromatin has already been

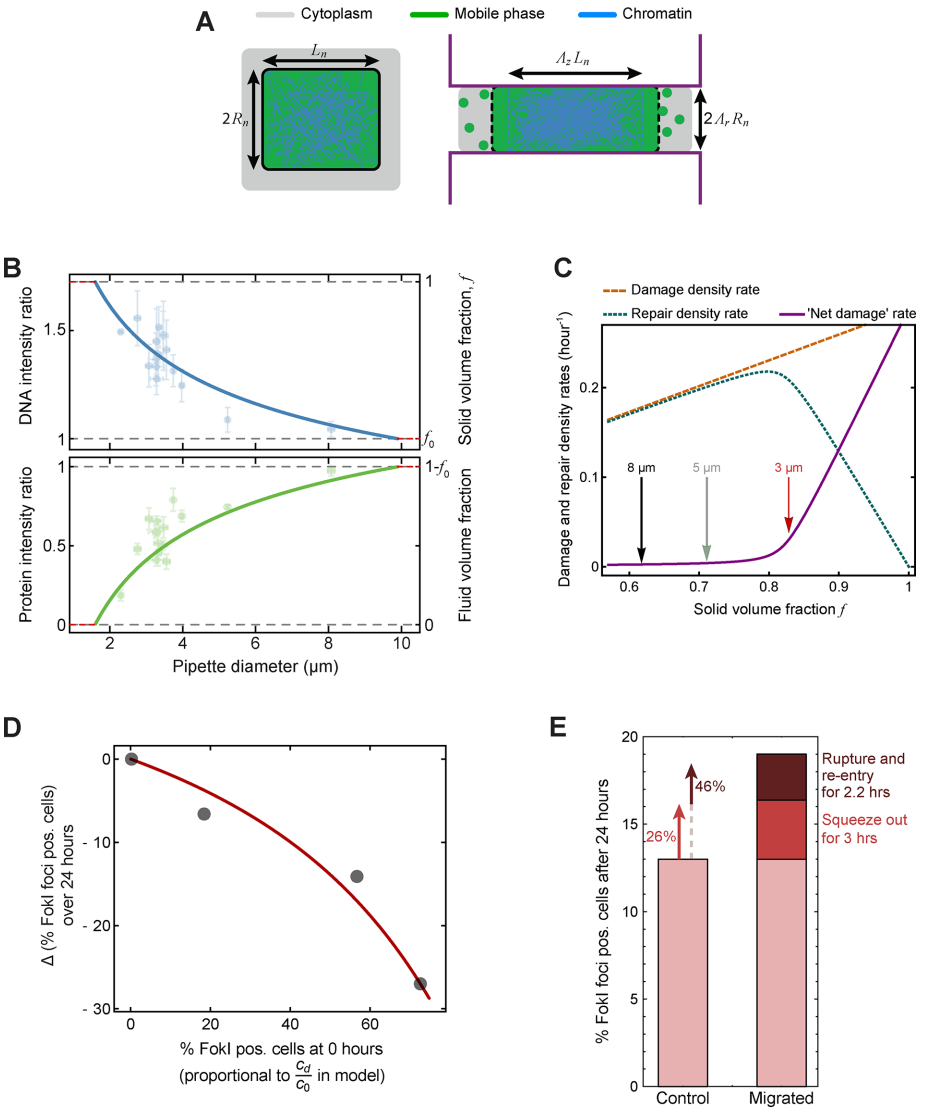

FIGURE 6: Elastic nucleus model of cell migration recapitulates mobile protein segregation and predicts that constriction can lower a cell's mutation rate by inhibiting nuclease activity. (A) Schematic illustrates chromatin compaction and key model parameters. In the model, the cell (shown here in side view) is treated as a cylinder with a cylindrical nucleus of radius R_n and length L_n. The nucleus consists of a solid chromatin mesh (blue) intermixed with a fluid of mobile nuclear proteins (green). When the nucleus is constricted, the chromatin squeezes out the protein fluid, as pictured, and the nuclear radius and length change by factors of Λ_r and Λ_z, respectively. (B) The model closely predicts the observed correlations between solid/fluid volume fractions and pipette diameter (compare with Figure 2C). Top, data points show the experimentally measured DNA intensity ratios for pipettes of different sizes. The blue curve reports the solid volume fraction f predicted by the theory, which relates to pipette size according to a power law. Bottom, data points give the protein intensity ratios measured using different-sized pipettes. The green curve is the predicted fluid volume fraction given by the same power law that determines the solid volume fraction in the top plot. At the critical pore size at which the fluid volume fraction vanishes, all of the fluid is squeezed away from the chromatin. We use this critical pore size to estimate the solid volume fraction of the undeformed nucleus to be $f_0 = 0.58$. (C) Damage, repair, and net damage density rates vary with the volume fraction f of the solid chromatin mesh, which increases upon constriction. These curves assume no added nuclease. The net rate is the difference between the damage and repair rates; it gives the number of unrepaired breaks per unit time, and the fitting used here shows those unrepaired breaks that lead to apoptosis. The arrows indicate the volume fractions corresponding to 8-, 5-, and 3-μm pores. (D) Higher nuclear FokI concentrations yield a higher percentage of FokI foci-positive cells at 0 h and, correspondingly, more burnout over 24 h. Gray points show experimental data. The percentage of FokI foci–positive cells at 0 h is proportional to the concentration of nuclease c_d/c_0; the bottom-right data point, representing the highest c_d/c_0, is used to estimate a proportionality constant in the model. The dark red curve shows the predicted burnout (i.e., change in percentage of FokI foci–positive cells) between 0 and 24 h, which increases in magnitude with percentage of FokI foci–positive cells at 0 h—and, by extension, with nuclease concentration. (E) Constricted migration delays burnout of the FokI-cleaved locus on chromosome 1 (compare with Figure 5E). We use the control bar, which reports the measured percentage of FokI foci–positive cells on top of the Transwell membrane after 24 h, to estimate the cells' nuclear FokI concentration. The total height of the migrated bar amounts to the measured percentage of FokI foci–positive cells on the bottom of the Transwell membrane after 24 h: the light pink portion gives the control value, the medium red portion shows the increase in foci-positive cells due to squeeze-out of FokI during the cells' 3-h-long migration through the 3-μm pores, and the dark red portion shows the increase in foci-positive cells due to mislocalization of FokI after migration-induced nuclear rupture. The model requires that FokI take ~2.2 h after rupture to relocalize to the nucleus in order to account for the specific observed increase in foci-positive cells after migration. The medium and dark red portions of the bar indicate that squeeze-out and rupture both play important roles in the difference in burnout observed between migrated and unmigrated cells.

estimated from mobility measurements to occupy roughly $f_0 \approx 65\%$ of the nuclear volume of a couple of adherent types of cells in static culture (Bancaud *et al.*, 2009), so that the free volume for diffusion of mobile factors is $(1 - f_0) \approx 35\%$. Our data show that a 3- to 4-μm constriction increases the local density of chromatin by a factor of ~1.3 (Figures 1B and 2B). Hence, inside the pore, $f_{\text{constricted}} \approx 84\%$, which causes the free volume there to decrease to $(1 - f_{\text{constricted}}) \approx 16\%$. It follows that mobile factors should deplete in the constriction to $(1 - f_{\text{constricted}})/(1 - f_0) \approx 45\%$ of their original abundance, which is in reasonable agreement with 3- to 4-μm pore and pipette measurements (Figures 1B and 2C).

Calculating squeeze-out and physical inhibition of nuclease attack

A more complete calculation uses the full range of pore size data (Figure 2C) to ultimately predict how much of the reduction in burnout of the locus in chromosome 1 (Figure 5E) occurs because of nuclease exclusion from the constriction (Figure 4, D and E) versus rupture into the cytoplasm

(Figure 4F). The cell is modeled as a cylinder of radius R_c encasing a cylindrical nucleus of radius R_n and squeezing into a cylindrical pore of radius $R_p < R_n$ (Figure 6A). When the nucleus is constricted in the radial direction, the solid mesh pushes the fluid outward; the change in fluid volume in the region surrounding the mesh depends on the change in volume of the region containing the mesh. As the nucleus is deformed, fluid is squeezed out, causing the solid volume fraction f to increase. From conservation of volume, the constricted volume is related to the initial volume by

$$f_{\text{constricted}} = \frac{f_0}{\Lambda_z \Lambda_r^2} \quad (1)$$

where Λ_r is the ratio of constricted to original nuclear radius and Λ_z is the ratio of constricted to original nuclear length (Figure 6A). Λ_z is related to Λ_r by a power law, $\Lambda_z = 1/\Lambda_r^{\alpha}$, $0 \le \alpha \le 2$, which is exact in the small-deformation limit. We fit to the DNA intensity data in Figure 2 to obtain $\alpha = 1.7$. Using this power- law, we fit to the protein intensity data to estimate the critical pore diameter of 1.6 µm at which all the fluid is squeezed out. We use these to estimate the initial solid volume fraction, $f_0 \approx 58\%$ (Figure 6B).

Our model incorporates f into a net damage density rate, k_m, which is the difference between a damage density rate, k_d, and a repair density rate, k_r, and, as such, defines the number of unrepaired DNA breaks per unit volume per unit time for a given cell (Figure 6C). The first term, k_d, is just the sum of a basal damage density rate and an induced damage density rate:

$$k_d = \kappa_d \left(f + \frac{c_d}{c_0}(1-f) \right) \quad (2)$$

where κ_d is a rate constant, c_d is the concentration of damage factor (i.e., nuclease) within the nucleus's mobile protein fluid, and c_0 is a constant to be fitted. The repair term, k_r, is derived from a Langmuir adsorption model—an equilibrium model that considers the adsorption and desorption rates of repair molecules from break sites. We use this model to predict the fraction of break sites f_r that adsorb a repair molecule during the time interval $\delta\tau$, which is set by a desorption rate parameter. The net damage density rate $k_n = k_d - k_r$ then becomes

$$k_n = k_d (1 - f_r) \quad (3)$$

with k_d given by Eq. 2. We fit the model parameters by setting $c_d = 0$ and comparing to apoptosis rates in rigid-pore migration experiments without added nuclease (Harada *et al.*, 2014). We have assumed that the apoptosis rate is proportional to DNA damage; more detailed observations of DNA damage would allow us to improve our estimate of the parameters and estimate a proportionality constant. Equation 3 is strictly a function of the solid volume fraction f and, by extension, of the nuclear deformation.

When there is no added nuclease ($c_d = 0$), an increase in nuclear deformation—and, with it, an increase in f—raises the net damage rate, as the squeezed-out repair molecules become unavailable to fix DNA breaks (Figure 6B). However, in the presence of added nuclease, deformation causes that nuclease to segregate and so inhibits its ability to inflict damage. If there is a large concentration of nuclease, then the decrease in damage during migration is more significant than the decrease in repair rate, so migration leads to appreciably less net damage. The relationship between nuclease concentration and corresponding damage (Figure 6D) shows that higher nuclease concentrations lead to a faster burnout rate, and the curve predicted by the model closely matches experimental data. The model ultimately predicts that squeeze-out of FokI accounts for more than half of the observed delay in burnout (i.e., increase in percentage of FokI foci–positive cells) after Transwell migration; the other half can be explained by nuclear rupture–induced FokI mislocalization (Figures 5E and 6E).

This predictive model provides insight into how an unavoidable physical consequence of constricted migration—namely, the squeeze-out of mobile nuclear proteins because of chromatin compaction—can have important functional consequences for the cell. Squeeze-out inhibits the net activity of the targeted nuclease. Similar segregation could also effectively separate the cell's repair factors from DNA damage sites in the constrictions, thereby causing elevated damage in migrating cells independent of nuclear envelope rupture.

MATERIALS AND METHODS

Cell culture

U2OS human osteosarcoma cells were cultured in DMEM high-glucose (Life Technologies, Carlsbad, CA) supplemented with 10% fetal bovine serum and 1% penicillin/streptomycin (Sigma-Aldrich, St. Louis, MO). Approximately 250 lac operator repeats (~9 kb per repeat) were integrated into the p-end of chromosome 1 of U2OS cells. Induction medium consisting of 4-hydroxytamoxifen (Sigma-Aldrich) and Shield1 ligand (Takara, Kusatsu, Japan) was then used to activate the integrated FokI-lac repressor-mCherry construct and induce DNA breaks, as described previously (Shanbhag *et al.*, 2010). A separate stable cell line of U2OS expressing YFP-NLS-MS2 was used and also described previously (Janicki *et al.*, 2004). Where used, protein overexpression was achieved by 24-h transfection with Lipofectamine 2000 (Life Technologies). Most of the expression plasmids were donated from various research groups, except for mApple-Fibrillarin and H2B-GFP, which were gifts from Michael Davidson (Florida State University; plasmid 54900; Addgene, Cambridge, MA) and Geoff Wahl (Salk Institute; Kanda *et al.*, 1998; plasmid 11680, Addgene), respectively. EC4 mouse liver cancer cells and A549 human lung cancer epithelial cells were cultured in supplemented DMEM high-glucose—with 1% MEM Non-Essential Amino Acids (Life Technologies)—and supplemented Ham's F12 medium (Life Technologies), respectively.

Transwell migration

Cells were plated on top of a Transwell membrane (Corning, Corning, NY) at a density of 300,000 cells/cm^2 and allowed to migrate to the bottom over the course of 24 h.

Immunostaining and imaging

Cells were fixed in 4% formaldehyde (Sigma-Aldrich) for 15 min before undergoing 10-min permeabilization by 0.25% Triton-X (Sigma-Aldrich), 30-min blocking by 5% bovine serum albumin (BSA; Sigma-Aldrich), and overnight incubation in primary antibodies. The antibodies used include lamin-A/C (Santa Cruz Biotechnology, Dallas, TX, and Cell Signaling, Danvers, MA), lamin-B (Santa Cruz Biotechnology), γH2AX (Millipore, Billerica, MA), 53BP1 (Abcam, Cambridge, UK), and acetylated histone H3 (K9 + K14 + K18 + K23 + K27; Abcam). The cells were then incubated in secondary antibodies (ThermoFisher, Waltham, MA) for 1.5 h, and their nuclei were stained with 8 µM Hoechst 33342 (ThermoFisher) for 15 min. Finally, the cells were mounted with Prolong Gold antifade reagent (Life Technologies). Epifluorescence imaging was done using an Olympus IX71—with a 40×/0.6 numerical aperture (NA) objective—and a digital electron-multiplying charge-coupled device (EMCCD) camera (Cascade; Photometrics, Tucson, AZ). Confocal imaging was done on a Leica TCS SP8 system equipped with either a 63×/1.4 NA

oil-immersion or a 40×/1.2 NA water-immersion objective. ImageJ (Schneider *et al.*, 2012) and MATLAB were used to quantify the resulting images.

Micropipette aspiration

In preparation for aspiration, cells were 1) detached using 0.05% trypsin-ethylenediaminetetraacetic acid (Life Technologies), 2) incubated in 0.2 μg/ml latrunculin A (Sigma-Aldrich) and 8 μM Hoechst 33342 (ThermoFisher) for 30 min at 37°C as described previously (Pajerowski *et al.*, 2007), and 3) resuspended in phosphate-buffered saline with 1% BSA and 0.2 μg/ml latrunculin A. During aspiration, epifluorescence imaging was done using a Nikon TE300—with a 60×/1.25 NA oil-immersion objective—and a digital EMCCD camera (Cascade, Photometrics). The resulting images were quantified in ImageJ (Schneider *et al.*, 2012).

Image analysis

During micropipette aspiration, the portion of the nucleus outside the pipette extends across a greater depth than does the portion inside. Thus, because epifluorescence signal is cumulative along the optical axis (*z* per Figure 1A), more photons are collected outside the pipette than inside, which artificially deflates the inside-to-outside intensity ratio. To correct for this effect, one can introduce a geometric factor α The chromatin's solid volume fraction *f* can then be written in terms of *a* as $f = [(1 - 1/ax)/(x - 1)]\ I_{ratio\_DNA}$, where I_{ratio_DNA} is the DNA intensity ratio and *x* is its maximum value. Similarly, the fluid volume fraction ρ can be expressed as $\rho = [(1 - 1/ax)/y]\ I_{ratio\_protein}$, where $I_{ratio\_protein}$ is the protein intensity ratio with maximum value *y*. Plugging these expressions into the relation $\rho = 1 - f$, it is straightforward to solve for $I_{ratio\_protein}$ as a function of I_{ratio_DNA}. DNA and protein intensity ratios prove to be negatively linearly correlated irrespective of the exact value of the geometric factor *a*. All plots with error bars are representative of mean ± SEM, and all statistical tests were done with a Student's *t* test.

Comet assay

Alkaline comet assays were performed according to manufacturer's protocol (Cell Biolabs, San Diego, CA).

ACKNOWLEDGMENTS

We thank Jiri Lukas (University of Copenhagen, Copenhagen, Denmark), Marc S. Wold (University of Iowa, Iowa City, IA), and Xiaochun Yu (University of Michigan, Ann Arbor, MI) for various DNA damage response protein plasmids used in this study, and also Jessica Zielinski (undergraduate from Clemson University) for valuable support in the FokI experiments. This work was supported by the National Cancer Institute of the National Institutes of Health under PSOC Award U54 CA193417. The content is solely the responsibility of the authors and does not necessarily represent the official views of the National Institutes of Health. This work was also partially supported by the National Science Foundation under Grant NSF-DMR-1506625 (R.R.B. and A.J.L.) and a Simons Investigator Award from the Simons Foundation to A.J.L.

REFERENCES

Bancaud A, Huet S, Daigle N, Mozziconacci J, Beaudouin J, Ellenberg J (2009). Molecular crowding affects diffusion and binding of nuclear proteins in heterochromatin and reveals the fractal organization of chromatin. EMBO J 28, 3785–3798.

Bekker-Jensen S, Lukas C, Melander F, Bartek J, Lukas J (2005). Dynamic assembly and sustained retention of 53BP1 at the sites of DNA damage are controlled by Mdc1/NFBD1. J Cell Biol 170, 201–211.

Clark RAF, Lanigan JM, DellaPelle P, Manseau E, Dvorak HF, Colvin RB (1982). Fibronectin and fibrin provide a provisional matrix for epidermal cell migration during wound reepithelialization. J Invest Dermatol 79, 264–269.

Dahl KN, Ribeiro AJ, Lammerding J (2008). Nuclear shape, mechanics, and mechanotransduction. Circ Res 102, 1307–1318.

Denais CM, Gilbert RM, Isermann P, McGregor AL, te Lindert M, Weigelin B, Davidson PM, Friedl P, Wolf K, Lammerding J (2016). Nuclear envelope rupture and repair during cancer cell migration. Science 352, 353–358.

Harada T, Swift J, Irianto J, Shin JW, Spinler KR, Athirasala A, Diegmiller R, Dingal PC, Ivanovska IL, Discher DE (2014). Nuclear lamin stiffness is a barrier to 3D migration, but softness can limit survival. J Cell Biol 204, 669–682.

Hass CS, Lam K, Wold MS (2012). Repair-specific functions of replication protein A. J Biol Chem 287, 3908–3918.

Hickson I, Zhao Y, Richardson CJ, Green SJ, Martin NM, Orr AI, Reaper PM, Jackson SP, Curtin NJ, Smith GC (2004). Identification and characterization of a novel and specific inhibitor of the ataxia-telangiectasia mutated kinase ATM. Cancer Res 64, 9152–9159.

Janicki SM, Tsukamoto T, Salghetti SE, Tansey WP, Sachidanandam R, Prasanth KV, Ried T, Shav-Tal Y, Bertrand E, Singer RH, Spector DL (2004). From silencing to gene expression: real-time analysis in single cells. Cell 116, 683–698.

Kanda T, Sullivan KF, Wahl GM (1998). Histone-GFP fusion protein enables sensitive analysis of chromosome dynamics in living mammalian cells. Curr Biol 8, 377–385.

Kurosaka S, Kashina A (2008). Cell biology of embryonic migration. Birth Defects Res C Embryo Today 84, 102–122.

Lamalice L, Le Boeuf F, Huot J (2007). Endothelial cell migration during angiogenesis. Circ Res 100, 782–794.

Li M, Yu X (2013). Function of BRCA1 in the DNA damage response is mediated by ADP-ribosylation. Cancer Cell 23, 693–704.

Lichtman MA (1970). Cellular deformability during maturation of the myeloblast. Possible role in marrow egress. N Engl J Med 283, 943–948.

Liotta LA, Steeg PS, Stetler-Stevenson WG (1991). Cancer metastasis and angiogenesis: an imbalance of positive and negative regulation. Cell 64, 327–336.

Luster AD, Alon R, von Andrian UH (2005). Immune cell migration in inflammation: present and future therapeutic targets. Nat Immunol 6, 1182–1190.

Nuciforo PG, Luise C, Capra M, Pelosi G, d'Adda di Fagagna F (2007). Complex engagement of DNA damage response pathways in human cancer and in lung tumor progression. Carcinogenesis 28, 2082–2088.

Pajerowski JD, Dahl KN, Zhong FL, Sammak PJ, Discher DE (2007). Physical plasticity of the nucleus in stem cell differentiation. Proc Natl Acad Sci USA 104, 15619–15624.

Petrie RJ, Koo H, Yamada KM (2014). Generation of compartmentalized pressure by a nuclear piston governs cell motility in a 3D matrix. Science 345, 1062–1065.

Pryde F, Khalili S, Robertson K, Selfridge J, Ritchie AM, Melton DW, Jullien D, Adachi Y (2005). 53BP1 exchanges slowly at the sites of DNA damage and appears to require RNA for its association with chromatin. J Cell Sci 118, 2043–2055.

Raab M, Gentili M, de Belly H, Thiam HR, Vargas P, Jimenez AJ, Lautenschlaeger F, Voituriez R, Lennon-Dumenil AM, Manel N, Piel M (2016). ESCRT III repairs nuclear envelope ruptures during cell migration to limit DNA damage and cell death. Science 352, 359–362.

Schneider CA, Rasband WS, Eliceiri KW (2012). NIH Image to ImageJ: 25 years of image analysis. Nat Methods 9, 671–675.

Shanbhag NM, Rafalska-Metcalf IU, Balane-Bolivar C, Janicki SM, Greenberg RA (2010). ATM-dependent chromatin changes silence transcription in cis to DNA double-strand breaks. Cell 141, 970–981.

Shin JW, Spinler KR, Swift J, Chasis JA, Mohandas N, Discher DE (2013). Lamins regulate cell trafficking and lineage maturation of adult human hematopoietic cells. Proc Natl Acad Sci USA 110, 18892–18897.

Tang J, Cho NW, Cui G, Manion EM, Shanbhag NM, Botuyan MV, Mer G, Greenberg RA (2013). Acetylation limits 53BP1 association with damaged chromatin to promote homologous recombination. Nat Struct Mol Biol 20, 317–325.

Thiam HR, Vargas P, Carpi N, Crespo CL, Raab M, Terriac E, King MC, Jacobelli J, Alberts AS, Stradal T, *et al.* (2016). Perinuclear Arp2/3-driven actin polymerization enables nuclear deformation to facilitate cell migration through complex environments. Nat Commun 7, 10997.

Ward IM, Minn K, van Deursen J, Chen J (2003). p53 binding protein 53BP1 is required for DNA damage responses and tumor suppression in mice. Mol Cell Biol 23, 2556–2563.